Comparative study of cross-sectional scanning tunneling microscopy/spectroscopy on III–V hetero- and homostructures: Ultrahigh vacuum-cleaved versus sulfide passivated

A. R. Smith and S. Gwo
Department of Physics, The University of Texas at Austin, Austin, Texas 78712

K. Sadra, Y. C. Shih, and B. G. Streetman
Department of Electrical and Computer Engineering, The University of Texas at Austin, Austin, Texas 78712

C. K. Shih
Department of Physics, The University of Texas at Austin, Austin, Texas 78712

(Received 2 March 1994; accepted 24 March 1994)

A comparative study of surfaces prepared by sulfide passivation and by UHV cleaving using cross-sectional scanning tunneling microscopy and spectroscopy (XSTM/S) is performed. Test samples used include both GaAs/(AlGa)As heterojunctions and GaAs *pn* junctions. Sulfide-passivated heterojunction surfaces allow much useful electronic information to be deduced from the tunneling spectroscopy since the tip-induced band bending problem is solved. Atomic resolution across UHV-cleaved heterojunctions allows a direct measurement of the asymmetrical interfacial roughness which agrees very well with the value deduced from tunneling spectroscopy on the sulfide-passivated surface. In the case of the UHV-cleaved *pn* junction surface, the tip-induced band bending effect is seen to manifest itself as a spatial shift in the conductivity profile within the depletion region. Sulfide-passivated *pn* junctions show a topographic profile which correlates very well with the secondary ion mass spectrometry profile, indicating that this technique is a potentially powerful dopant profiling method. Each type of prepared surface possesses its own advantages and disadvantages which are discussed. In particular, we address the manifestation of the tip-induced band bending effect in the tunneling spectroscopy.

I. INTRODUCTION

For many years, researchers have been studying semiconductor heterojunctions and homojunctions with the aim of fully understanding their structural and electronic properties. Almost since the invention of scanning tunneling microscopy (STM), intensive effort has been applied to utilize cross-sectional scanning tunneling microscopy and spectroscopy (XSTM/S) for studying these structures.[1–16] Due to the localized nature of the tunneling probe, STM showed promising potential for mapping out the detailed structural and electronic properties across semiconductor interfaces with very high resolution. Using a combination of scanning electron microscopy (SEM) (to locate the junctions) and STM, Salemink and co-workers demonstrated the first atomic resolution images across GaAs/(AlGa)As heterojunctions.[1,2] More recent results by Johnson *et al.* have shown the ability to resolve individual dopant sites and local alloy fluctuations.[3,4] However, obtaining accurate measurements of electronic properties such as band offsets turned out to be difficult when it was realized that the tip-induced band bending effect was a serious problem.[2] Thought to be due to depletion of carriers at the interfaces, this effect resulted in a measurement error on the same order as the band offset itself (0.1–0.2 eV). Thus this problem was considered a limitation on the technique of XSTM/S, particularly in the case of large band gap semiconductors.

In our earlier work,[5] we have demonstrated the ability to overcome the tip-induced band bending problem by utilizing a sulfide-passivation technique. On a sulfide-passivated cross-sectional surface, accurate measurements were obtained for: (1) the band offsets, (2) the asymmetrical transition widths, and (3) the multiple-valley band thresholds. It was found that the sulfide-passivation technique produced a sample surface with a uniformly pinned Fermi level, thus reducing the tip-induced band bending. The advantages of having a pinned surface were also discussed by Feenstra in a study of *pn* junctions in which the surface was highly stepped.[6] However, the sulfide-passivation technique provides a controllable method of producing such a surface, enabling highly repeatable measurements. This is then an extremely useful method since it allows the deduction of so much information in such a convenient manner.[7] On the other hand, if atomically resolved structural information is desired, studying the UHV-cleaved surface is essential. But then, one has to take into account the unavoidable influence of tip-induced band bending.

The objective of this investigation is to make some comparisons between uniformly pinned surfaces prepared using an $(NH_4)_2S$ passivation technique and partially pinned or unpinned surfaces prepared by cleaving in UHV. On the one hand, we would like to understand how the tip-induced band bending effect manifests itself on UHV-cleaved surfaces, particularly in the tunneling spectroscopy. This is done by making a comparison with results from a pinned surface. Such an understanding will then help us to deduce accurate electronic information, even in the presence of tip-induced band bending. On the other hand, we want to know how structural information, such as interfacial roughness, derived

 0734-211X/94/12(4)/2610/6/$1.00

from atomically resolved images, correlates with that obtained indirectly through the tunneling spectroscopy.

For the purposes of this study, we focus on two model semiconductor systems: GaAs/(AlGa)As heterojunctions and GaAs multiple *pn* junctions. Currently the two most commonly used surface preparation techniques for these sample systems, sulfide passivation and UHV cleaving both offer distinctly different advantages as indicated.

II. EXPERIMENT

The experiments are performed inside a UHV chamber having a base pressure of less than 6×10^{-11} Torr. For positioning the tip within the epilayer region, the STM is equipped with a high-precision dual-axis sample translation stage. Tips are prepared by electrochemically etching polycrystalline tungsten wires and then cleaning them in UHV using a field emission method on clean substrates. Samples are grown using molecular-beam epitaxy (MBE) on (001) oriented wafers with Si and Be used as dopants.

Individual samples are prepared for cleavage by scribing a mark on the epilayer surface with a diamond pen. In the case of the passivation method, immediately (within a few seconds) after cleaving the sample *ex situ*, it is immersed in a sulfide $(NH_4)_2S$ solution.[8] We want to point out that another type of sulfur passivation has been used by Dagata *et al.*[9] After passivating for about 5–10 min, the sample is rinsed in de-ionized water and blown dry with nitrogen gas. It is then mounted in a sample holder and loaded into the UHV chamber by means of a sample load lock. In the case of the UHV-cleaved samples, the cleaving is performed by pushing the sample along the $[00\bar{1}]$ direction.

The techniques used for locating the epilayer region have been described in detail elsewhere.[10,11] Electronic information is obtained by performing detailed spectroscopy measurements across the electrical junctions of interest. One spectroscopy curve is obtained for each point of a 64×64 pixel area where the points are distributed uniformly within the total scan area. At each point, the STM feedback loop is interrupted, the tip position is held fixed, the spectrum is acquired, and the feedback loop is turned on again. Simultaneously, a topographic image is acquired, allowing a direct comparison of structural and electronic information.

III. RESULTS AND DISCUSSION

A. GaAs/(AlGa)As heterojunctions

From our previous investigations on sulfide-passivated GaAs/(AlGa)As heterojunction surfaces, we have found that it is possible to deduce useful electronic information from the tunneling spectroscopy $I-V$ curves by calculating the conductivity quantity $d\ln I/dV$.[5] A similar method of analyzing the spectroscopy data has been used by Feenstra *et. al.*[6,12] In Fig. 1, we show a plot of the quantity $d\ln I/dV$ as a function of position and sample bias with the corresponding STM image of sulfide-passivated heterojunctions shown below. This method of treating the data has the following advantages. First, being inversely proportional to $V-V_0$, this quantity is highly sensitive to the band edge position V_0. As seen in the plot, the data shows the expected $1/(V-V_0)$ be-

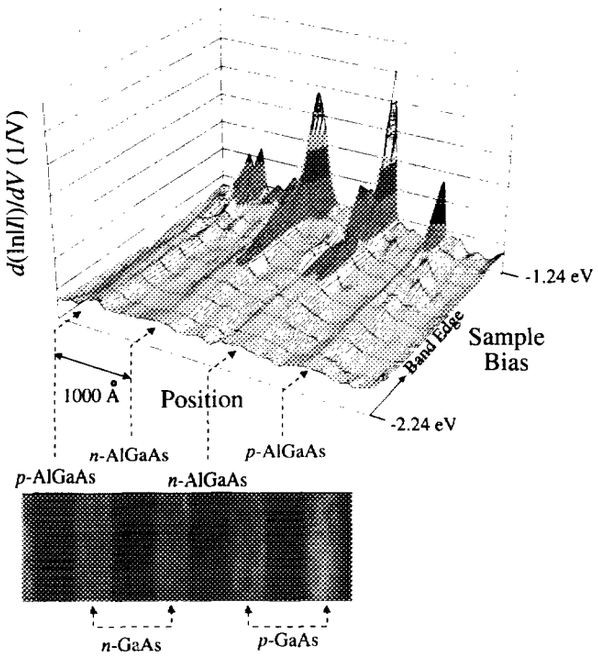

FIG. 1. A plot of normalized conductivity $d\ln I/dV$ vs position and sample bias over a scanning area of 4500 Å×1500 Å. The corresponding STM image acquired at a sample bias of −2.35 V and a tunneling current of 0.3 nA is displayed in the lower left corner.

havior. The second advantage is what is particularly important in the study of junctions where the electronic effect results in quite a large tip-sample separation difference as one moves across the junction. Calculating $d\ln I/dV$ removes this exponential dependence, making it possible to obtain sensitivity on both sides of the junction. In this way, it becomes very convenient to map out the spatial variation of the electronic properties across junctions. Moreover, the band edge position relative to the Fermi level can then be derived, enabling band offset values to be determined. It is important to note that the pinning of the surface Fermi level due to the sulfide passivation has the result of minimizing the tip-induced band bending effect but does not alter the band offset values.

The method of $d\ln I/dV$ is very nice for determining not only band offsets but also the asymmetric interfacial roughness. This roughness manifests itself as a difference in the electronic transition width λ_t of the "normal" [(AlGa)As grown on top of GaAs] interface compared to the "inverted" [GaAs grown on top of (AlGa)As] interface. Shown in Fig. 2(a) is a topographic image where the light region is GaAs and the dark regions are (AlGa)As. Tunneling spectroscopy is performed at each pixel in the image, and from this, the quantity $d\ln I/dV$ is calculated. These values are then averaged along the vertical direction and plotted versus x in Fig. 2(b). From this, the valence-band maximum (VBM) position is calculated and plotted versus x in Fig. 2(c) which shows the band offset. A fitting procedure is then applied to individual VBM profiles at different positions along the $[\bar{1}10]$

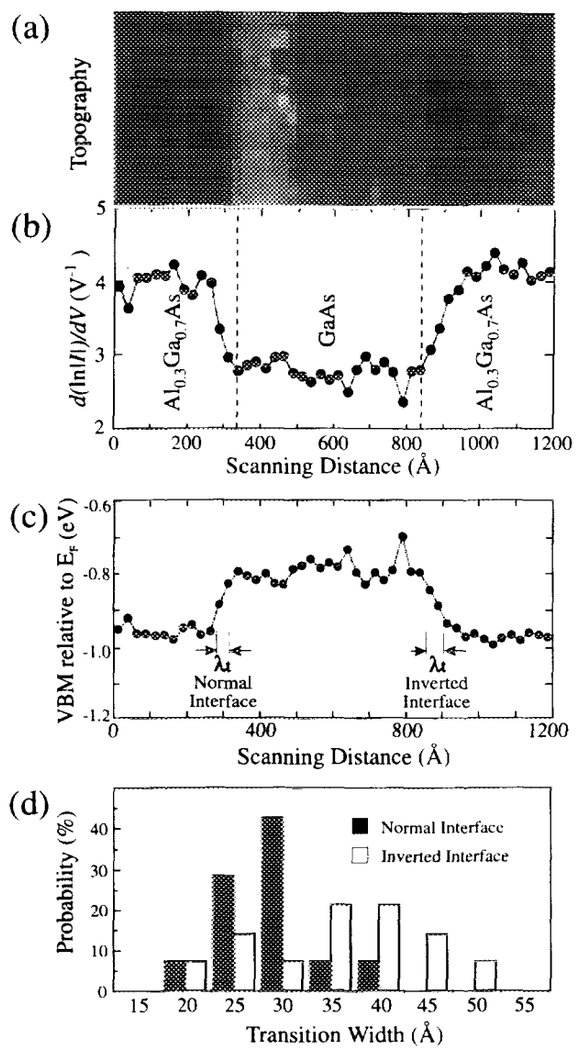

FIG. 2. (a) A 48×21 pixel STM image in which I–V spectra were taken at each pixel in the image, (b) the plot of $d \ln I/dV$ vs position at negative sample bias (−1.59 V), (c) the positions of valence-band edges (referenced to the Fermi level) vs position, and (d) a histogram of transition widths for normal (full bar) and inverted (open bar) interfaces.

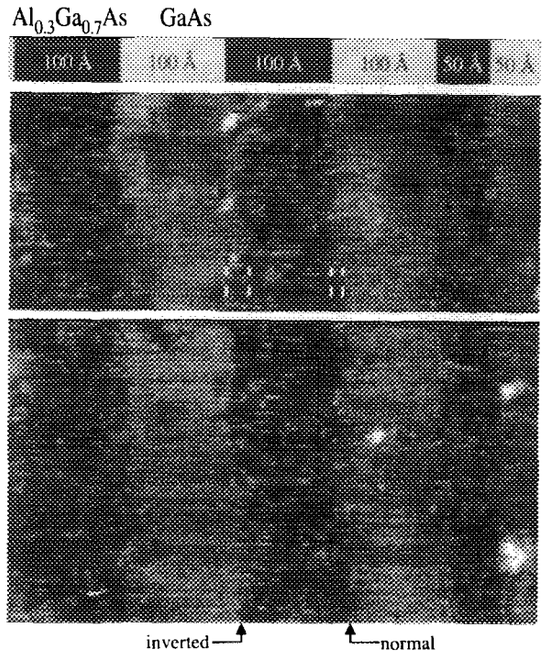

FIG. 3. A 500 Å × 500 Å atomic resolution STM image of $GaAs/Al_{0.3}Ga_{0.7}As$ heterojunctions taken at a sample bias of −2.34 V and a tunneling current of 0.3 nA, showing the existence of alloy ordering and asymmetric interfacial roughness which is marked by the dashed lines.

direction, and the transition widths are derived.[5] These results are presented in the histogram shown in Fig. 2(d). As can be seen, for the normal interface, the average is about 30 Å while the average for the inverted interface is about 40 Å, a difference of about two lattice constants. However, we expect the actual interfacial roughness value to be smaller than that derived from the tunneling spectroscopy due to tailing in of the wavefunctions.

A determination of the true interfacial roughness requires atomic resolution data across the heterojunctions, namely, data on the UHV-cleaved surface. Such data are provided in Fig. 3, where we show a 500 Å×500 Å atomic resolution filled state image of the UHV-cleaved cross-sectional surface of $GaAs/Al_{0.3}Ga_{0.7}As$ heterojunctions. This image was acquired with a sample bias of −2.34 V and a tunneling current of 0.3 nA. One clearly sees atomic rows running along the [$\bar{1}$10] direction inside the GaAs regions and the presence of interfacial roughness at the atomic scale. Atomic scale interfacial roughness has been previously observed by Johnson *et al.*, but the asymmetry was not discussed.[13,14] However, in our study, the interfacial roughness at the inverted interface is greater than that at the normal interface by about two atomic rows, as marked in the figure. This value agrees quite well with that calculated from the tunneling spectroscopy as measured on the sulfide-passivated surface, providing additional confirmation for the practicality of analyzing the spectroscopy data using the method of plotting $d \ln I/dV$ and also for the use of the sulfide-passivation treatment.

We now turn to a discussion of the tunneling spectroscopy on the UHV-cleaved heterojunction surface. Previous work by Salemink *et al.* directly observed the valence-band offset but not the conduction-band offset. This was attributed to the tip-induced band bending problem.[2] In our study, when stabilizing the tunneling junction on filled states (that is, with negative sample polarity), we have found similar contrast in the $d \ln I/dV$ plot for the valence band as that observed on sulfur-passivated surfaces, reflecting the effect of the valence-band offset. However, we do not observe a consistent contrast in the $d \ln I/dV$ plot for the conduction band. One may interpret this behavior as due to the tip-induced band bending effect such as that observed in the work of Salemink *et al.*[2] On the other hand, a lot of our tunneling spectroscopy data were acquired while stabilizing the tunneling junction on empty states (conduction band). In this case,

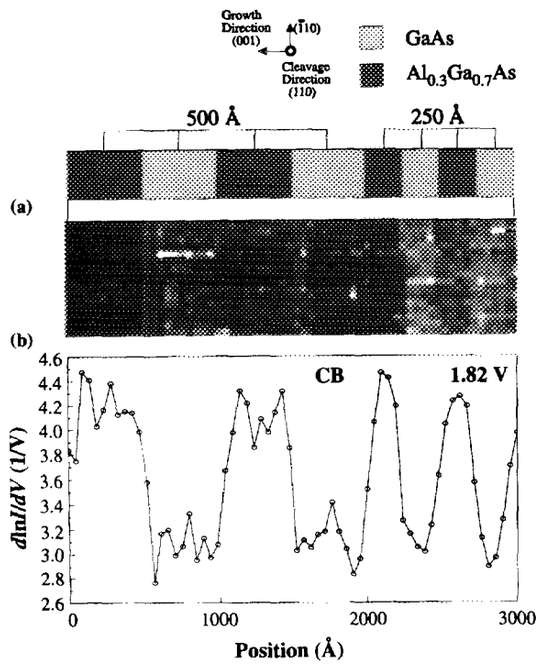

FIG. 4. (a) A 3000 Å×250 Å image of $GaAs/Al_{0.3}Ga_{0.7}As$ heterojunctions acquired at a sample bias of +2.18 V and a tunneling current of 0.16 nA. The topographic contrast does not correlate with the conduction-band conductivity profile shown in (b) most likely due to the existence of steps. The conductivity profile does, however, clearly delineate the 500- and 250-Å wide regions.

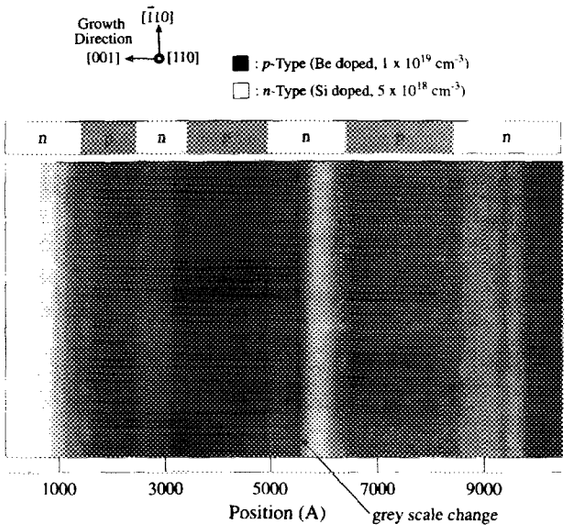

FIG. 5. Mosaic STM image (each acquired at sample bias of −2.63 V and a tunneling current of 0.2 nA) of a UHV-cleaved GaAs *pn* junction surface showing steps primarily within the *n*-type regions. The total area shown is about 10 500 Å by 5000 Å, and the grey scale range is about 6.5 Å for the image on the right and 9.7 Å for the image on the left. These two are separated by the very sharp line running down the middle.

when we analyze the data by calculating $d \ln I/dV$, we find that the conductivity profile does reflect the existence of the conduction-band offset but not the valence-band offset.

In Fig. 4(a), we present an example of a 3000 Å×1000 Å STM image together with its corresponding device structure. It is important to note in this image that the light and dark regions do not correlate with the actual structure, most likely due to the presence of steps. However, the assignment of the regions is straightforward after plotting the conductivity profile, shown in Fig. 4(b), and comparing it with the grown device structure. Based upon the conductivity difference between the junctions, the estimated conduction-band offset is about 0.14–0.18 eV. This value is slightly lower than what we obtained on the sulfide-passivated surface of about 0.22 eV.[5]

We believe the difficulty in obtaining valence- and conduction-band offsets simultaneously in UHV-cleaved samples is a direct result of tip-induced band bending. It appears that the sensitivity to the band offset in the conduction band or the valence band is directly related to the polarity of the feedback stabilization voltage. Stabilizing the feedback on the occupied states of the sample often results in good sensitivity to the valence-band offset while stabilizing on the unoccupied states often results in good sensitivity to the conduction-band offset.

While it appears that the tip-induced band bending effect is an important factor in the case of GaAs/(AlGa)As, it is not necessarily of major importance in other sample systems. In this case of GaAs/(AlGa)As, the magnitudes of the band offsets to be measured are on the same order as the magnitude of the tip-induced band bending effect. But in other systems with smaller band gaps, the error introduced by the tip-induced band bending effect is greatly reduced, such as is the case for the InAs/GaSb system as reported by Feenstra.[15]

B. GaAs multiple *pn* junctions

Figure 5 shows a large scale mosaic image of the UHV-cleaved (110) surface of a GaAs multiple *pn* junction sample. The device structure consists of repeated periods of alternating *p*- and *n*-type regions having the following widths: 2000 Å (*n*)−2000 Å (*p*)−1500 Å (*n*)−1500 Å (*p*)−1000 Å (*n*)−1000 Å (*p*) when going from right to left in the picture. Nominally, the *p*-type regions are doped 1×10^{19} cm^{-3} [Be] while the *n*-type regions are doped 5×10^{18} cm^{-3} [Si]. This results in an abrupt junction depletion width of about 250 Å. The assignment of the width and doping of the layers in this image can be achieved by comparing the topographic features and the conductivity profiles with the expected device structure.

Figure 6(a) shows a 4500 Å×800 Å STM image of the same surface with the normalized conductivity $d \ln I/dV$ plotted versus position in Fig. 6(b) for both the valence and conduction bands. Since the conductivity is inversely proportional to the difference between the tip Fermi level and the band edge, the conduction-band conductivity should be larger in *p*-type regions while the valence-band conductivity should be larger in *n*-type regions. Comparing the topographic features and the conductivity profiles, we conclude that the central dark region in this image is *p*-type and that the lighter stepped-looking regions are *n*-type. Similar con-

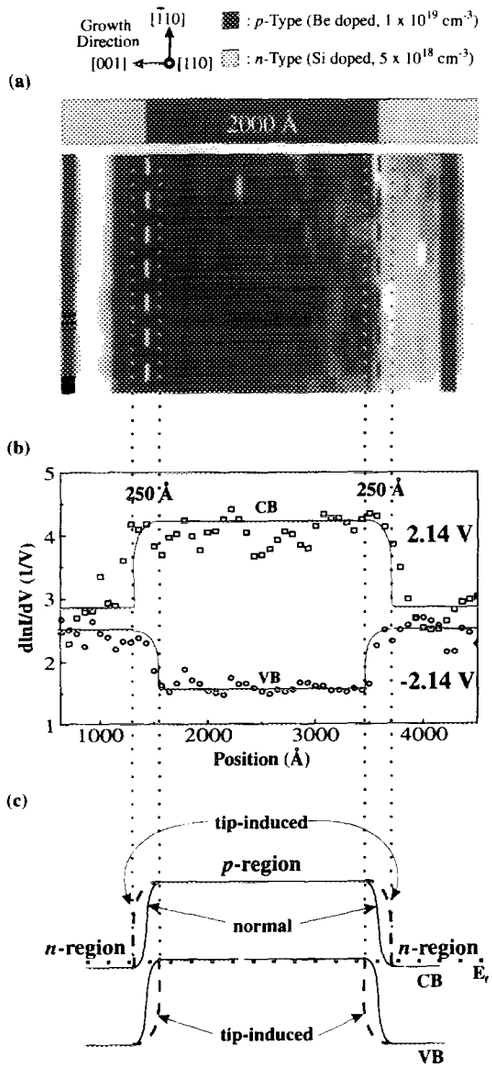

FIG. 6. (a) A 4500 Å×800 Å STM image of a UHV-cleaved GaAs *pn* junction region taken at a sample bias of −2.72 V and a tunneling current of 0.18 nA and, (b) the corresponding conduction-band and valence-band conductivity profiles revealing the existence of a spatial shift at the junctions of about 250 Å, consistent with the depletion width for an abrupt junction. In (c) is shown the band structure model illustrating the effect of tip-induced band bending within the depletion region.

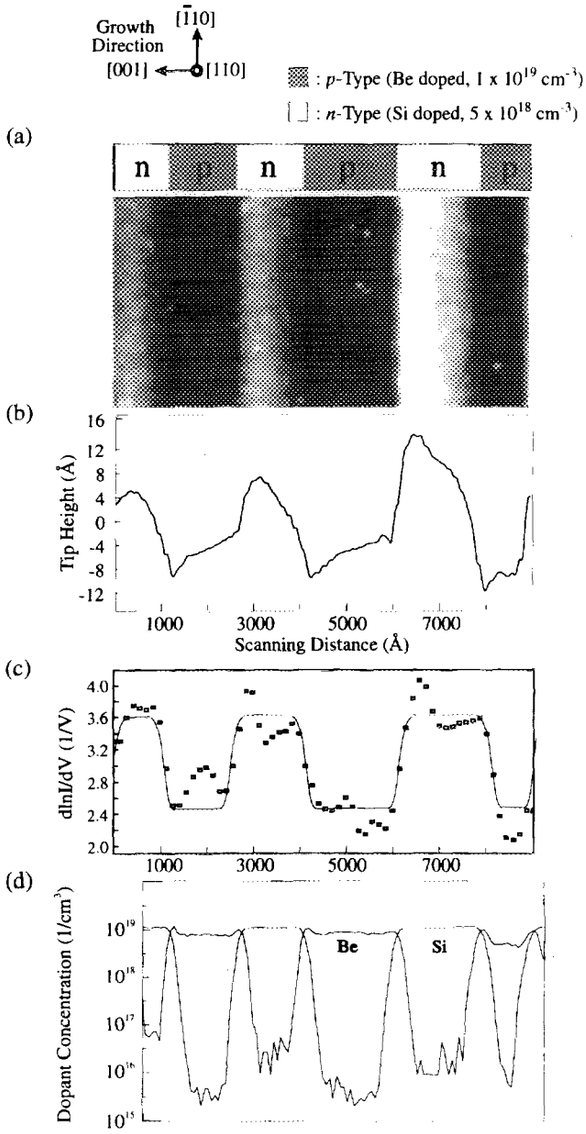

FIG. 7. (a) A 9000 Å×800 Å constant current STM image of sulfide-passivated *pn* junctions acquired at a sample bias of −2.14 V and a tunneling current of 0.17 nA clearly showing the delineation of *n* and *p* regions and (b) the corresponding topographic profile which correlates very well with (c) the valence-band conductivity profile. The asymmetry seen in (b) indicates the existence of dopant diffusion within the device which is confirmed with the SIMS profile shown in (d).

trast was observed in our earlier UHV-cleaved *pn* junction work.[16] The formation of steps predominantly within the *n*-type regions appears to be a common rule for most of the cleaved surfaces that we have studied, resulting in a weak pinning of the Fermi level in those regions.

The valence- and conduction-band conductivity profiles exhibit a spatial shift relative to each other which has a magnitude consistent with the calculated depletion width. We believe that this shift is due to band bending within the depletion region. To understand how such a shift occurs, we consider the effect of the tip-induced electric field on the bands within the depletion region. Shown in Fig. 6(c) is the expected band structure for this region shown in solid lines. Within the depletion regions, the tip-induced electric field causes the conduction band to be pulled upward and the valence band to be pulled downward. The result is that the apparent widths of the conductivity profiles change, giving rise to the observed spatial shift.

The results for the UHV-cleaved surface may be directly compared with the results for the sulfide-passivated surface of a sample taken from the same wafer and thus the same device structure. In Fig. 7(a), a 9000 Å by 800 Å STM image of the passivated *pn* junction surface is shown in which the

n- and *p*-type regions are clearly delineated. Also, the conductivity profile shown in Fig. 7(c) correlates very well with the topographic linecut shown in Fig. 7(b).

Secondary ion mass spectrometry (SIMS) analysis was also performed on this same sample, and the results are shown in Fig. 7(d). The result reveals an asymmetrical Be concentration within the *p*-type regions which slopes upward toward the left with small peaks at both edges, the peak on the left-hand side being larger than the peak on the right-hand side, as displayed in the image. These features correlate extremely well with the topographic profile. Where the Be concentration is larger, the tip pushes in further, and this shows up as dips in the topography corresponding to peaks in the SIMS profile. This correlation is highly consistent.

In contrast to the UHV-cleaved surface, the apparent topographic contrast is much larger on the passivated sample with *n*- and *p*-type regions differing by as much as 26 Å. There are several possible explanations for this large contrast. One is that this is a dopant selective etching effect. In this case, we must conclude that the etching proceeds faster where there is the largest Be concentration. Another possibility, however, is that this is an effect of the surface states which pin the Fermi level. These states form a surface charge layer which compensates the space charge region underneath, the total charge being directly related to the doping density. The surface charge layer modifies the tunneling barrier height and thus the tunneling probability. The result is the apparent topographic height difference which we observe. The true cause of the contrast mechanism will require further investigation. A combined STM/AFM study would be useful. Nevertheless, regardless of the contrast mechanism, the correlation between the STM topography and the dopant distribution as revealed by the SIMS analysis is astonishing. We have then a technique with potential for use as a two-dimensional dopant profiling tool.

IV. CONCLUSION

We have studied GaAs/(AlGa)As heterojunction and GaAs multiple *pn* junction samples with XSTM/S using both sulfide passivation and UHV-cleaving sample preparation techniques with the aim of making a comparative study between the two. For the sulfide-passivated heterojunction surface, we find that the Fermi level is pinned uniformly, making possible the deduction of much useful electronic information such as band offsets and multiple band thresholds. However, only the UHV-cleaved heterojunction surface has the advantage of providing atomically resolved information. The directly measured interfacial roughness asymmetry does in fact confirm that derived from the tunneling spectroscopy on the passivated surface. For the UHV-cleaved *pn* junction surface, the tip induced band bending effect manifests itself as a spatial shift in the conductivity profile, and the magnitude of the shift is consistent with the depletion width. For the sulfide-passivated *pn* junction surface, on the other hand, the correlation between the STM topography and the dopant distribution as revealed by SIMS analysis suggests that this technique has potential for performing two-dimensional dopant profiling.

ACKNOWLEDGMENTS

This work was supported by the Texas Advanced Research Program, the Trull Centennial Professorship in Physics Fellowship No. 1, the Joint Services Electronics Program (No. AFOSR F49620-92-C-0027), and a grant from the Army Research Office (No. DAAL03-91-G-0034).

[1]O. Albrektsen, D. J. Arent, H. P. Meier, and H. W. M. Salemink, Appl. Phys. Lett. **57**, 31 (1990).
[2]H. W. M. Salemink, O. Albrektsen, and P. Koenraad, Phys. Rev. B **45**, 6946 (1992).
[3]M. B. Johnson, O. Albrektsen, R. M. Feenstra, and H. W. M. Salemink, Appl. Phys. Lett. **63**, 2923 (1993).
[4]M. B. Johnson, H. P. Meier, and H. W. M. Salemink, Appl. Phys. Lett. **63**, 3636 (1993).
[5]S. Gwo, K.-J. Chao, C. K. Shih, K. Sadra, and B. G. Streetman, Phys. Rev. Lett. **71**, 1883 (1993).
[6]R. M. Feenstra, A. Vaterlaus, E. T. Yu, P. D. Kirchner, C. L. Lin, J. M. Woodall, and G. D. Pettit, *Semiconductor Interfaces at Sub-Nanometer Scale*, NATO ASI Series E No. 243, edited by H. W. M. Salemink and M. D. Pashley (Kluwer, Dordrecht, 1993), p. 127.
[7]S. Gwo, K.-J. Chao, C. K. Shih, K. Sadra, and B. G. Streetman, Appl. Phys. Lett. **64**, 493 (1994).
[8]S. Gwo, A. R. Smith, K.-J. Chao, C. K. Shih, K. Sandra, and B. G. Streetman, J. Vac. Sci. Technol. A **12**, 2005 (1994).
[9]J. A. Dagata, W. Tseng, J. Bennett, J. Schneir, and H. H. Harary, Appl. Phys. Lett. **59**, 3288 (1991); Ultramicroscopy, **42**, 1288 (1992).
[10]S. Gwo, K.-J. Chao, A. R. Smith, C. K. Shih, K. Sadra, and B. G. Streetman, J. Vac. Sci. Technol. B **11**, 1509 (1993).
[11]The authors acknowledge useful discussions with S. F. Alvarado concerning the edge-finding algorithm.
[12]A. Vaterlaus, R. M. Feenstra, P. D. Kirchner, J. M. Woodall, and G. D. Pettit, J. Vac. Sci. Technol. B **11**, 1502 (1993).
[13]M. B. Johnson, U. Maier, H.-P. Meier, and H. W. M. Salemink, Appl. Phys. Lett. **63**, 1273 (1993).
[14]H. W. M. Salemink and O. Albrektsen, Phys. Rev. B **47**, 16 044 (1993).
[15]R. M. Feenstra, D. A. Collins, D. Z.-Y Ting, M. W. Wang, and T. C. McGill, J. Vac. Sci. Technol. B **12**, 2592 (1994).
[16]S. Gwo, A. R. Smith, C. K. Shih, K. Sadra, and B. G. Streetman, Appl. Phys. Lett. **61**, 1104 (1992).